

## $^{40}\text{Ar}$ – $^{39}\text{Ar}$ Ages of Rocks and Glasses from the Nördlinger Ries Crater and the Temperature History of Impact Breccias

Th. Staudacher<sup>1</sup>, E.K. Jessberger, B. Dominik, T. Kirsten, and O.A. Schaeffer<sup>2\*</sup>

Max-Planck-Institut für Kernphysik, 6900 Heidelberg, Federal Republic of Germany

**Abstract.** We report on a  $^{40}\text{Ar}$ – $^{39}\text{Ar}$  study of hornblende, biotite, and glass samples from the Nördlinger Ries impact crater. The samples are derived from various depths (377–1,200 m) of the Forschungsbohrung 1973 drill core, from the ejecta blanket, and the crystalline crater rim. All mineral separates display  $^{40}\text{Ar}$ – $^{39}\text{Ar}$  plateau ages of  $320 \pm 3$  m.y. The data represent the first direct age determination of the Ries bedrock. The plateau ages of suevite and moldavite, both generated in the Ries impact, date the cratering event which occurred 15 m.y. ago. The results from the mineral separates imply that shock pressure alone, even as high as 450 kbar, cannot reset K–Ar ages of hornblende and biotite. This result is significant for the interpretation of ages of impact breccias in general, and for the interpretation of lunar highland rock ages in particular.

$^{40}\text{Ar}$ – $^{39}\text{Ar}$  studies yield, as a side result, data on the natural loss of radiogenic  $^{40}\text{Ar}$ . In this report we emphasize on this aspect to estimate the cooling history of the suevite layer. We compare the measured  $^{40}\text{Ar}$ -loss to the loss calculated from a simple cooling model of the layer and from the diffusion properties of the minerals as obtained in the stepwise heating experiment. The resulting upper limit for the post-shock equilibrium temperature within the suevite layer is  $450^\circ\text{C}$ .

**Key words:** Radioactive dating – Suevite – Impact breccia – Cooling history – Nördlinger Ries – Forschungsbohrung 1973 – Lunar samples

### Introduction

In the early state of the solar system, meteorite impacts have fundamentally altered the surfaces of planetary bodies. On the moon, collisions gave rise to the formation of the enormous lunar ring basins and to sculpturing the lunar highlands. The relative sequence of the formation of basins can be established by photogeological means. The absolute time scales can be inferred by radiometric dating of lunar rocks, mainly using the  $^{40}\text{Ar}$ – $^{39}\text{Ar}$  dating method (Jessberger et al., 1974; Kirsten and Horn, 1975; Turner, 1977).

In dating a lunar impact breccia which is normally produced in a sequence of multiple impacts, it is necessary to evaluate the response of the parent-daughter isotope system to shock pressure, to the accompanying temperature rise during the impact, and to the heat exposure after burial and compaction within hot ejecta blankets.

The preponderance of certain age values in lunar highland chronology suggests that a complete resetting of the K–Ar clock may have occurred during the formation of large lunar ring basins (Schaeffer et al., 1976). Elevated temperatures – either before the impact at some depth or after the impact within thick hot ejecta blankets –, heating during the impact process or shock effects could all, in principle, be responsible. However, in many cases multiple “local” impacts rather than one single basin-forming event determine the age patterns (Kirsten and Horn, 1975; Horn and Kirsten, 1977). This became particularly evident from the consortium study of highland breccias 73215 and 73255 (James and Blanchard, 1976; James et al., 1978). These breccias were most probably produced in the Serenitatis basin-forming event (Ryder and Wood, 1977; Higuchi and Morgan, 1975), but nevertheless display a wide range of ages of individual components (Jessberger et al., 1976, 1977, 1978b; Staudacher et al., 1979), all exceeding the age of the only two dated clasts which were definitely molten during breccia compaction (James et al., 1978; James and Hammarstrom, 1977). Only these exceptional felsite clasts date the age of basin formation (Jessberger et al., 1978b; Staudacher et al., 1979), all other breccia constituents have not been completely reset at this occasion, but rather have retained records of their per-basin history.

Clearly, a systematic investigation of the influence of large impacts on the K–Ar system of the rocks involved in the impact is urgently needed. Our approach is to use the best documented terrestrial giant meteorite impact, the Nördlinger Ries crater event, for a case study of these effects.

The 24 km-Ries crater was formed 15 m.y. ago (Gentner et al., 1961) possibly by a stony meteorite (El Goresy and Chao, 1977). To study the vertical structure of the crater (Fig. 1), a 1,206 m deep drill core was obtained in 1973. A detailed description of the drill core is given by Gudden (1974) and Schmidt-Kaler (1977).

From 0 to 324 m depth, post-Ries lake sediments cover a suevite breccia layer (324–601 m). The latter can be divided into a high temperature layer (324 m–525 m depth) and a low temperature layer (525 m–602 m depth). The two suevite layers are distinguished in that the content of molten glass is higher in the upper layer (Bauburger et al., 1974; Stöffler et al., 1977). On the other hand, the low temperature layer is characterized by

1 *Present address.* Université de Paris 6 et 7, Laboratoire de Géochimie et Cosmochimie, 4, place Jussieu, F-75230 Paris Cedex 05, France

2 *Permanent address.* Dept. of Earth and Space Sciences, State University of New York, Stony Brook, NY 11794, USA

\* O.A. Schaeffer died on November 11, 1981

*Reprint requests to.* T. Kirsten, Max-Planck-Institut für Kernphysik, Postfach 103980, 6900 Heidelberg, Federal Republic of Germany

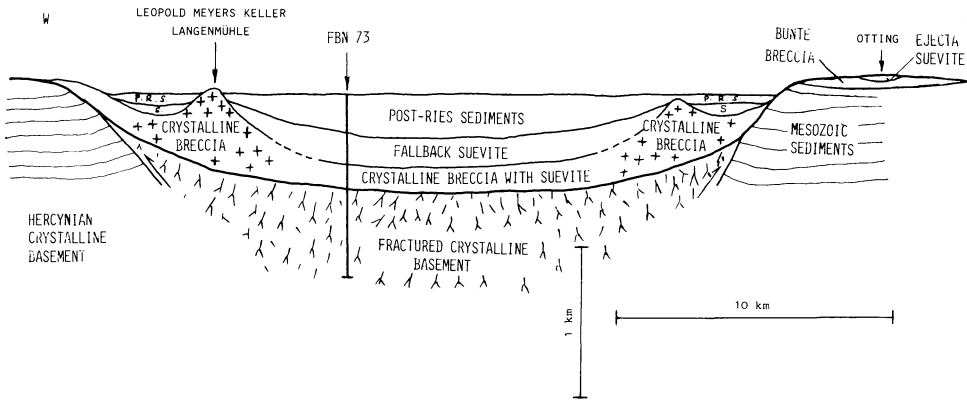


Fig. 1. Schematic cross section through the Nördlinger Ries crater (G. Wagner, unpublished). Note the difference between horizontal and vertical scales

the frequent occurrence of crystalline rock fragments and blocks. Below the crater floor at 602 m (El Goresy and Chao, 1977), mainly crystalline bedrock can be found. Near the crater floor, the bedrock is highly fractured as a result of shock waves but fracturing decreases with depth. At 1,200 m depth, the rock is almost undisturbed.

## Experimental

### Samples

Amphibolites and gneisses have been selected for our  $^{40}\text{Ar}$ - $^{39}\text{Ar}$  study. They represent all major drill core units and occur as fragments and blocks in suevite and as massive basement rocks:

- 1) amphibolite (401 m) and gneiss (503 m) as fragments from the high temperature suevite;
- 2) blocks of hornblende gneiss (571 and 585 m) from the low temperature suevite;
- 3) amphibolites (603 and 637 m) from the compressed zone of the crystalline basement rocks;
- 4) gneiss (1,201 m) from the drill core bottom, representing undisturbed crystalline basement rock.

In addition, we have prepared and studied a sample of the high temperature (377 m) suevite, a gneiss fragment from the fallout suevite breccia of the "Otting" locality and an amphibolite from the crystalline crater wall at "Meyer's Keller".

Hornblende and biotite were separated using heavy liquids and magnetic separation. Chlorite enriched samples have also been prepared. In the following, they are designated by the term chlorite. Care was taken to preserve the natural grain sizes of the minerals as far as possible in order to prevent bias in the degassing properties if the in situ situation is compared to the laboratory situation. Some crushing is unavoidable in the preparation of mineral separates, therefore, the finest size fraction has been rejected from analysis.

For sample identification, we assign code symbols H for hornblende, B for biotite, C for chlorite mineral separates and G for glasses. The code letter is followed by the sample depth expressed in meters or by the symbols MK for Meyer's Keller or O for Otting.

The samples display a wide range of shock-generated alterations. The latter imply impact pressures ranging from < 10 kbar up to 500 kbar (Table 3). This was determined by microscopic and SEM investigations applying criteria as established by Stöffler (1971, 1972).

**401 m – Amphibolite.** The mineral assemblage (plagioclase, hornblende, chlorite, biotite, opaques) is typical of a plagioclase-rich

amphibolite. A thin section reveals a granoblastic texture with a wide range of grain sizes (5  $\mu\text{m}$ –3 mm; average 100–400  $\mu\text{m}$ ). Plagioclase occurring as anhedral grains is strongly altered into sericite. Prismatic, anhedral or subhedral hornblende grains as well as biotite are chloritized. Chlorite in this amphibolitic fragment is not always an alteration product of mafic phases. Instead, it also occurs as large primary single crystals or flaky, sometimes subrounded aggregates which may be as large as 3 mm in size.

The amphibolite is weakly shocked (pressure < 100 kbar). The primary structure is deformed by common intergranular microfractures and by parallel planar intergranular fractures of hornblende. Sericitization of plagioclase and chloritization of mafic minerals may have been promoted by shock in some cases, but more often they appear to be due to diaphoretic decomposition induced by tectonic forces (Graup, 1977).

**503 m – Gneiss.** This hornblende gneiss fragment is composed of plagioclase, biotite, hornblende, quartz, and accessory constituents such as sphene, apatite, and opaque phases. Grain sizes range from 50  $\mu\text{m}$  to 2 mm. As in metamorphic Ries rocks, plagioclase is sericitized and biotite is chloritized. This rock shows the highest degree of shock among all fragment samples selected by us from the drill core. All quartz and some feldspar grains show planar elements. Biotite grains are strongly kinked, some are oxidized. The presence of planar elements in plagioclase indicates the shock pressure to exceed 150 kbar.

**570 and 585 m – Gneisses.** These gneisses are composed of hornblende, plagioclase, quartz, and the accessories sphene and opaques. Mineral grain sizes range from 40  $\mu\text{m}$ –3 mm (average size: 100–500  $\mu\text{m}$ ). The main constituents are hornblende and strongly sericitized plagioclase. Quartz is present in small amounts relative to feldspar. It forms single grains and veins oriented concordantly with the schistosity. Opaque phases are relatively abundant. Shock-produced, parallel oriented intergranular fractures are present. Minute branching microfractures are rare and visible in single grains only. Twins in plagioclase are often displaced by shear. Hornblende and quartz often show planar fractures. The above shock deformations suggest pressures of 100–150 kbar, confirming previous observations of von Engelhardt and Graup (1977) for this part of the drill core.

**603 and 637 m – Amphibolites.** These amphibolites from the compressed zone (El Goresy and Chao, 1977) are weakly shocked. They consist mainly of hornblende and plagioclase. Quartz, chlorite, opaques, sphene, and apatite are accessory. The whole rock as well as the single crystals are strongly fractured. Hornblende shows typical planar microfractures visible in most of the grains.

Quartz is usually damaged by inter- and intragranular microfractures. Plagioclase grains are deformed only by intergranular fractures. This distortion of the primary structure was produced by a pressure  $\leq 100$  kbar.

*1,201 m – Gneiss.* Microscopic examination shows compositional and structural features characteristic for gneiss. The rock consists of sericitized plagioclase, quartz, chlorite with biotite relicts and hornblende (grain size: 15  $\mu\text{m}$ –1.5 mm; average 200–400  $\mu\text{m}$ ). The only visible shock features are shock bands in biotite, suggesting that the deforming pressure did not exceed 10 kbar.

*Meyer's Keller – Amphibolite.* From the crystalline crater wall a shocked amphibolite has been studied. It consists mainly of hornblende and glass (grain size 400  $\mu\text{m}$ –2 mm). A high degree of shock is indicated by complete isotropisation of plagioclase. There is no relation between phases and flow structures, suggesting that the transformation took place in the solid state. The glass is diaplectic. Hornblende grains are distinctly lighter in colour than non-shocked hornblende in general. Pleochroism is reduced. Planar fractures are still present. Strong oxidation is due to shock-induced heating. The shock effects suggest that the amphibolite was subjected to shock pressure of 300–400 kbar.

*Otting – Gneiss.* The collected gneiss fragment from the fallout suevite "Otting" is composed of glass, biotite, and hornblende. Sphene and apatite are accessory, but relatively abundant minerals (grain size 20  $\mu\text{m}$ –2.5 mm; average 200  $\mu\text{m}$ ). The gneiss fragment displays highly non-uniform shock effects. Part of the specimen is moderately deformed by a peak pressure of  $\sim 400$  kbar. As is the case for the specimen from Meyer's Keller, plagioclase and quartz are totally isotropized without melting. The biotite shows strong kinking and is partly oxidized. The colour of the hornblende is unusually light. Another part of the same fragment is appreciably more deformed, corresponding to a pressure of 400–450 kbar. The glass consists of liquid state plagioclase glass with flow structure and vesicles and of solid state quartz glass with coesite. Such transitions from moderately to strongly

**Table 1.** Consistency of Bern 4 Muskovite and NL25,2 hornblende monitors. The established K–Ar age of NL25,2 is  $2,660 \pm 9$  m.y. (Schaeffer and Schaeffer, 1977). Errors are  $1\sigma$

| Sample         | $^{40}\text{Ar}/^{39}\text{Ar}$ | Age (m.y.)            |
|----------------|---------------------------------|-----------------------|
| B4M $\pm 9$    | $5.203 \pm 0.012$               | $\equiv 18.5 \pm 0.2$ |
| B4M $\pm 10$   | $5.180 \pm 0.014$               | $\equiv 18.5 \pm 0.2$ |
| NL25,2 $\pm 5$ | $1,761.2 \pm 9.2$               | $2,709 \pm 19$        |
| NL25,2 $\pm 6$ | $1,752.6 \pm 9.0$               | $2,702 \pm 19$        |
| B4M $\pm 11$   | $5.216 \pm 0.013$               | $\equiv 18.5 \pm 0.2$ |
| B4M $\pm 12$   | $5.195 \pm 0.012$               | $\equiv 18.5 \pm 0.2$ |

**Table 2.** Summary of conversion factors  $C_K^{39}$  and correction factors for Ca and K derived argon isotopes for irradiations K1–K4/76 and K1+K2/77. Errors are  $1\sigma$

| Irradiation Number | Irradiation Time (h)      | $(^{36}\text{Ar}/^{37}\text{Ar})_{\text{Ca}} \times 10^{-4}$ | $(^{38}\text{Ar}/^{37}\text{Ar})_{\text{Ca}} \times 10^{-4}$ | $(^{39}\text{Ar}/^{37}\text{Ar})_{\text{Ca}} \times 10^{-4}$ | $(^{38}\text{Ar}/^{39}\text{Ar})_{\text{K}} \times 10^{-4}$ | $C_K^{39} (10^{-6} \text{ cc(STP)}^{39}\text{Ar/gK})$ |
|--------------------|---------------------------|--|--|--|---|---|
| K1/76              | 24 }<br>8 }<br>8 }<br>8 } | $2.9 \pm 0.2$  | $6.3 \pm 2.4$  | $8.4 \pm 0.2$  | $134 \pm 2$   | $13.88 \pm 0.03$                                      |
| K2/76              |                           |  |  |  |   | $4.44 \pm 0.04$                                       |
| K3/76              |                           |  |  |  |   | $4.71 \pm 0.07$                                       |
| K4/76              |                           |  |  |  |   | $4.16 \pm 0.15$                                       |
| K1/77 }<br>K2/77 } | 12                        | $3.1 \pm 0.2$  | $16.0 \pm 4.8$   | $10.7 \pm 0.3$   | $156 \pm 4$   | $5.86 \pm 0.06$<br>$6.04 \pm 0.13$                    |

shocked microareas are not unusual. Typically, they result from refraction and interference of shock waves.

#### $^{40}\text{Ar}$ – $^{39}\text{Ar}$ Dating

*Monitor and Irradiation.* For dating lunar and meteoritic samples we generally use the NL25,2 hornblende standard (Schaeffer and Schaeffer, 1977) with an  $^{40}\text{Ar}/^{40}\text{K}$  atom ratio of  $0.3530 \pm 0.0022$  and a K–Ar age of  $2.660 \pm 0.009$  AE, based on the newly recommended decay constants and K isotopic composition (Steiger and Jäger, 1977). Since the Ries crater is comparatively young,  $\sim 15$  m.y., NL25,2 is not an appropriate monitor and we therefore used the Bern 4 Muskovite (B4M) standard (Jäger, 1969). B4M has been analyzed in eleven laboratories, yielding an average  $^{40}\text{Ar}/^{40}\text{K}$  ratio of  $(1.080 \pm 0.006) \times 10^{-3}$  corresponding to a K–Ar age of  $18.5 \pm 0.2$  m.y. We compared B4M to NL25,2 in a separate irradiation (K1/76). The capsule was irradiated in the FR2-reactor in Karlsruhe, Germany, in a position which should have the least n-flux gradient along the sample ampoule. The measured  $^{40}\text{Ar}/^{39}\text{Ar}$  ratios and the ages of the NL25,2 samples calculated relative to B4M are listed in Table 1 in the same sequence as the samples were stacked in the ampoule. Relative to B4M, the K–Ar age of NL25,2 has been reproduced reasonably well. The constancy of the  $^{40}\text{Ar}/^{39}\text{Ar}$  ratios of the four B4M samples indicates that the neutron flux gradient is below 0.5% along the 4 cm linear dimension of ampoule K1/76. The uncertainty introduced by the neutron flux gradient for this irradiation is smaller than the statistical uncertainty of the isotope ratios. The result also demonstrates the high precision achievable in  $^{40}\text{Ar}$ – $^{39}\text{Ar}$  dating even in a case as unfavourable as here, when the  $^{40}\text{Ar}/^{39}\text{Ar}$  ratios of monitor and samples differ by a factor of  $\sim 350$ .

The Ries samples were irradiated in five different irradiations, K2–K4/76 and K1+K2/77. K2–K4/76 ampoules were not placed in the same position as K1/76. Instead, they were stacked on top of each other, separated by an empty capsule. In all irradiations  $\text{CaF}_2$  was also included. The resulting correction factors for Ca- and K-derived argon isotopes are listed in Table 2. The ratios  $C_K^{39} = \frac{^{39}\text{Ar}}{\text{K}} \frac{\text{cc(STP)}}{\text{g}}$  as measured by B4M monitors are different in each ampoule, indicating a neutron flux gradient. For the age calculation of Ries samples no neutron flux gradient correction has been applied since only two B4M monitors had been included in each ampoule because of space limitations. Instead, the average  $C_K^{39}$ -value for each ampoule has been assigned an error which covers the measured extremes and is given in Table 2.

#### Experimental Procedures

Before irradiation the samples were wrapped in high purity Al-foil. Muskovite decrepitates at about  $850^\circ\text{C}$ , as indicated by

**Table 3.** Summary of  $^{40}\text{Ar}$ - $^{39}\text{Ar}$  results for hornblende, biotite, chlorite, and glass samples from the Nördlinger Ries. The plateau range gives the fraction of  $^{39}\text{Ar}$  that defines the plateau in the age spectrum. The shock wave pressure is estimated by microscopic examination of thin sections following criteria given by Stöfler (1971, 1972)

| Position   |  | K    | $^{40}\text{Ar}_{\text{rad}}$ | $^{40}\text{Ar}_{\text{atm}}$ | K-Ar age       | $^{40}\text{Ar}$ - $^{39}\text{Ar}$<br>plateau age | Plateau<br>range | $^{40}\text{Ar}_{\text{rad}}$ loss | shock wave<br>pressure |
|--|--|------|-------------------------------|-------------------------------|----------------|--|------------------|------------------------------------|------------------------|
|  |  | (%)  | ( $10^8 \text{cc(STP)/g}$ )   | (%)                           | (m.y.)         | (m.y.)   | (%-%)            | (%)                                | (kbar)                 |
| <b>Ejecta</b>  |  |      |                               |                               |                |  |                  |                                    |                        |
| HMK  | amphibolite                              | 0.50 | 692                           | 3.3                           | $318 \pm 11$   | $321.6 \pm 10.6$                                   | 3- 98            | 0.5                                | 300-400                |
| HO   | gneiss<br>(suevite)                      | 0.51 | 675                           | 11.0                          | $274 \pm 5$    | $310.8 \pm 4.8$                                    | 24- 94           | 12.9                               | 400-450                |
| BO   |  | 4.15 | 5,200                         | 3.3                           | $296 \pm 6$    | $323.2 \pm 1.9$                                    | 24-100           | 8.9                                | 400-450                |
| <b>Core above the crater bottom</b>                  |  |      |                               |                               |                |  |                  |                                    |                        |
| B377   | suevite breccia                          | 1.89 | 2,421                         | 4.2                           | $302 \pm 3$    | $322.9 \pm 2.4$                                    | 22-100           | 7.0                                | n.d.                   |
| H401   | amphibolite<br>(suevite)                 | 0.92 | 1,181                         | 3.5                           | $275 \pm 3$    | $308.8 \pm 3.0$                                    | 16- 75           | 5.8                                | < 100                  |
| B401   |  | 3.61 | 4,514                         | 30.1                          | $296 \pm 5$    | -  | -                | -                                  | < 100                  |
| C401   |  | 0.50 | 625                           | 28.8                          | $293 \pm 7$    | $325.9 \pm 3.4$                                    | 28-100           | 10.8                               | < 100                  |
| B503   |  | 3.95 | 4,322                         | 2.2                           | $262 \pm 5$    | $322.0 \pm 2.0$                                    | 59-100           | 20.1                               | 150-250                |
| H570   | gneiss<br>(suevite)                      | 0.70 | 1,059                         | 3.6                           | $323 \pm 10$   | $323.2 \pm 10.5$                                   | 3-100            | 0.2                                | 100-150                |
| H585   |  | 0.71 | 881                           | 5.1                           | $269 \pm 6$    | $319.6 \pm 5.4$                                    | 18- 98           | 16.2                               | $\leq 100$             |
| <b>Core below the crater bottom, compressed zone</b> |  |      |                               |                               |                |  |                  |                                    |                        |
| H603   | amphibolite<br>(crystalline<br>basement) | 0.32 | 462                           | 3.7                           | $316 \pm 5$    | $317.4 \pm 4.9$                                    | 5- 99            | 0.3                                | $\leq 100$             |
| H637   |  | 0.81 | 1,134                         | 4.2                           | $315 \pm 3$    | $317.0 \pm 2.8$                                    | 2- 92            | 1.1                                | $\leq 100$             |
| <b>Undisturbed crystalline bedrock</b>               |  |      |                               |                               |                |  |                  |                                    |                        |
| H1201  | gneiss<br>(crystalline<br>basement)      | 0.67 | 949                           | 3.5                           | $319 \pm 4$    | $321.5 \pm 3.7$                                    | 9- 99            | 1.2                                | < 10                   |
| C1201  |  | 0.77 | 1,106                         | 7.7                           | $320 \pm 15$   | $323.5 \pm 6.2$                                    | 3-100            | -                                  | < 10                   |
| <b>Glass samples</b>                                 |  |      |                               |                               |                |  |                  |                                    |                        |
| GO   | suevite breccia                          | 2.68 | 166                           | 30.0                          | $15.0 \pm 0.3$ | $14.98 \pm 0.49$                                   | 3- 92            | -                                  | molten                 |
| GM   | moldavite                                | 2.76 | 160                           | 22.8                          | $15.2 \pm 0.2$ | $15.21 \pm 0.15$                                   | 12-100           | -                                  | molten                 |

H = hornblende; B = biotite; C = chlorite; G = glass; MK = Meyer's Keller; O = Otting; Numerals indicate the depth in the deep drill core

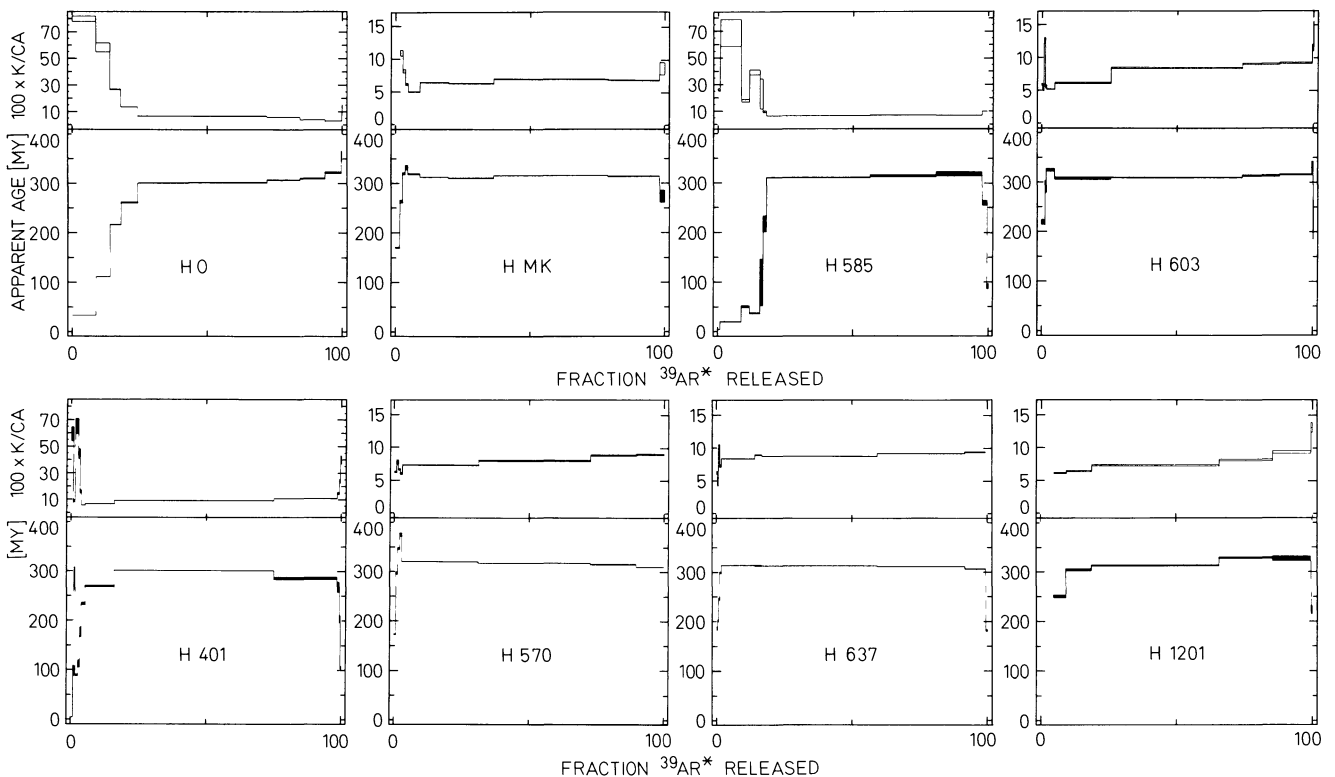


**Fig. 2.**  $^{40}\text{Ar}$ - $^{39}\text{Ar}$  age spectra for eight hornblende mineral separates from the Nördlinger Ries. For sample identification see Table 3

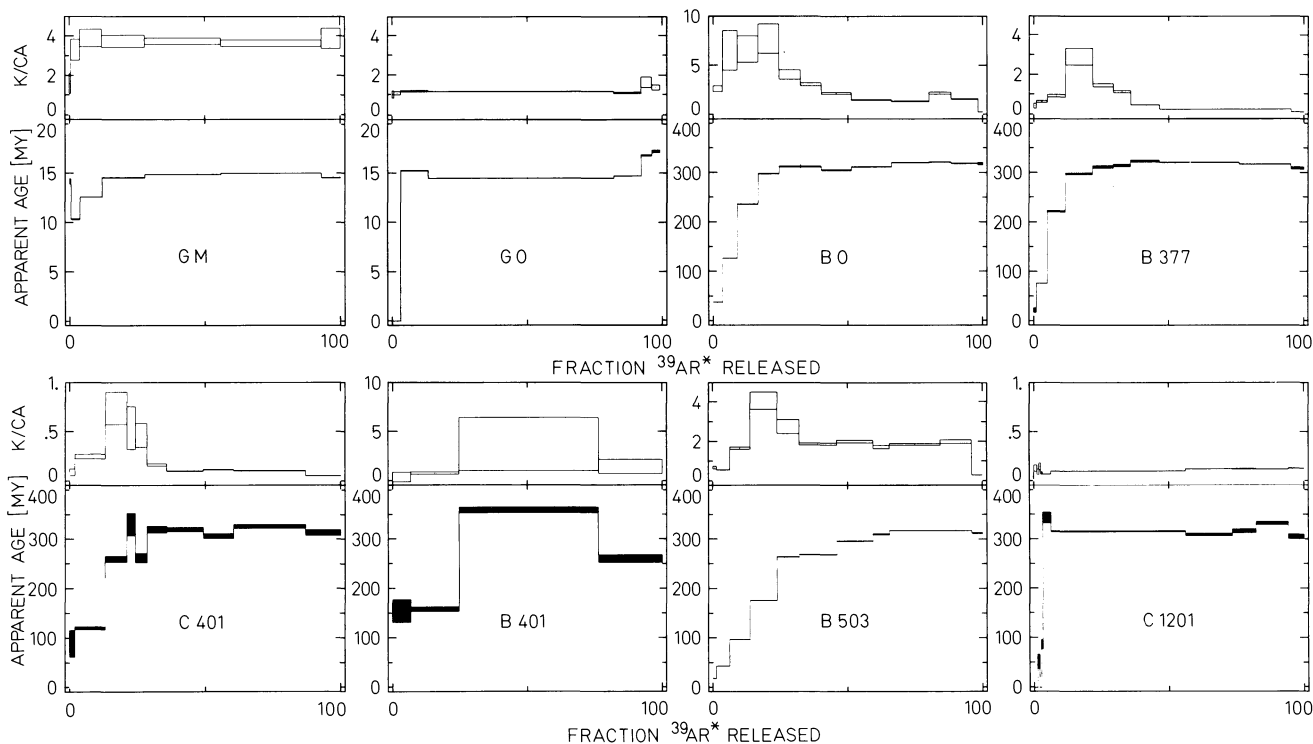


Fig. 3.  $^{40}\text{Ar}$ - $^{39}\text{Ar}$  age spectra for glass and chlorite and biotite mineral separate samples. For sample identification see Table 3

the high pressure of about 1 Torr in the extraction line at this temperature. To prevent sparking in the furnace, the B4M samples were wrapped in Au-foil before being loaded into the extraction system. Extraction temperatures for the mineral separate samples range from 400–1,500° C and up to 1,900° C for the moldavite and the suevite glass samples. Cooling of the extraction furnace between temperature fractions is usually avoided. The evolved gas was gettered over Ti at 750° C during extraction. Further purification was achieved by a Ti-getter which cooled from 750° C to room temperature, and by a pair of SAES getters.

Data acquisition, reduction, and correction followed our previously described routine (Jessberger et al., 1976). The voluminous individual argon isotopic data may be obtained from the first author on request.

#### Age and K/Ca Spectra

In Table 3 the  $^{40}\text{Ar}$ - $^{39}\text{Ar}$  data for the mineral separates and glass samples are compiled. The corresponding age and K/Ca spectra are shown in Figs. 2 and 3.

**Hornblende.** All age spectra of hornblende separates have age plateaux at about 320 m.y., extending over 3–5 release fractions and comprising 60–95% of the total of  $^{39}\text{Ar}$  released. The K-contents range between 0.3 and 0.9%.

In the age plateau regions of all hornblende samples the K/Ca ratios are also rather constant with an average value of 0.08. Only two spectra show clear evidence for losses<sup>1</sup> of radiogenic  $^{40}\text{Ar}$ , namely samples HO and H585. The losses are correlated with high K/Ca ratios of up to 0.7 and are therefore most probably not to be associated with hornblende but with a high K-contaminant. The nominal  $^{40}\text{Ar}$ -losses from the other samples, mostly less than 1.5%, are regarded as insignificant. The higher loss from H401, 5.8%, which is also accompanied by

initially high K/Ca ratios, is taken as the upper limit since the K-Ar age also includes the relatively young high temperature ages (Fig. 2). The primary result from these samples, apart from the inferred plateau age, is the observation that hornblende has essentially lost *no*  $^{40}\text{Ar}$  in the course of the Ries impact.

**Biotite and Chlorite.** The biotite and chlorite samples (except B401) also have age spectra with plateaux at ~320 m.y. The age plateaux comprise 4–8 fractions and represent 41–97% of the total  $^{39}\text{Ar}$ . The spectra are typical of samples which have lost portions of their radiogenic  $^{40}\text{Ar}$  after their formation. Nominal  $^{40}\text{Ar}$  losses range from 7%–20%.

The K/Ca-ratios of biotite show greater variations and are much higher than for hornblende. The average K/Ca value is ~0.7. B401 has a disturbed age pattern which may be artificial and due to the low sample weight, 4.9 mg, and the atmospheric  $^{40}\text{Ar}$  content of more than 30%. Nevertheless, the (total) K-Ar age of B401, 296 m.y., is only slightly lower than the average biotite plateau age of ~320 m.y. While the K-contents of biotite show normal values between 1.9 and 4.2%, the K-contents of “chlorite” are too high, which indicates that our samples are not pure chlorite.

**Glass Samples.** The age spectra of the moldavite (GM) and the suevite glass from Otting (GO) are shown in Fig. 3. The moldavite has a broad age plateau at 15.2 m.y. and includes four temperature fractions which comprise 88% of the  $^{39}\text{Ar}$ . GO has an age of 15.0 m.y. Unfortunately, this sample degassed 69% of the whole  $^{39}\text{Ar}$  in the 1,200° C fraction.

#### Discussion

The glass samples dated, GM and GO, both yield the age of the Ries event,  $15.1 \pm 0.1$  m.y. which had already been determined much earlier by conventional K-Ar dating (Gentner et al., 1961) and by fission track dating (Gentner et al., 1969).

1 The nominal  $^{40}\text{Ar}$ -losses are calculated from the total K-Ar ( $t_{\text{tot}}$ ) and plateau ( $t_{\text{pl}}$ ) ages by  $^{40}\text{Ar}_{\text{loss}} = 100 \times [1 - (e^{-\lambda t_{\text{tot}}}) - 1] / (e^{-\lambda t_{\text{pl}}} - 1)$

**Table 4.** Diffusion parameters,  $Q$  and  $B_0 = D_0 \pi^2 / a^2$ , and maximum post-shock temperatures,  $T_{ini}$ , obtained for mineral separate samples from the Nördlinger Ries. Sample nomenclature is the same as in Table 3. The last column gives the extraction temperature of the first plateau fraction

| Sample | Activation energy $Q$ (kcal/mol) | $B_0^a$ [s <sup>-1</sup> ] | $T_{ini}$ [°C] | $T_{plat}$ [°C] |
|--------|----------------------------------|----------------------------|----------------|-----------------|
| HMK    | 78.5 ± 2.2                       | 1 (8)–3 (8)                | 600–620        | 770             |
| HO     | 42.9 ± 2.8                       | 1 (3)–4 (3)                | 470–550        | 940             |
| BO     | 38.8 ± 2.0                       | 4 (2)–8 (3)                | 420–470        | 780             |
| B377   | 64.0 ± 5.2                       | 1 (6)–4 (7)                | 380–460        | 800             |
| H401   | 99.7 ± 6.1                       | 8 (10)–2 (12)              | 640–700        | 1,020           |
| C401   | 57.5 ± 3.4                       | 2 (5)–9 (5)                | 450–510        | 780             |
| B503   | 50.3 ± 2.2                       | 3 (4)–6 (4)                | 410–450        | 1,000           |
| H570   | 124.5 ± 5.2                      | 1 (16)–2 (17)              | 590–630        | 830             |
| H603   | 130.9 ± 6.1                      | 2 (17)–8 (18)              | 700–740        | 930             |

<sup>a</sup> 1 (8) = 1 · 10<sup>8</sup>

The average of all plateau ages obtained for the mineral separates is 320 ± 3 m.y. This includes the ages of the lower-most samples, H1201 and C1201, which are almost unaffected by the impact. The data represent the first direct age determination of the Variscan pre-Ries bedrock. Apparently no geologic event has totally reset the K–Ar clocks in these rocks in the last 320 m.y., even though the upper samples from the suevite layer had been involved in the turbulent and vigorous cratering process. Independent of the degree of shock features we find the ubiquitous 320 m.y. plateau age for all samples which were not totally molten as a result of the impact. This confirms and generalizes our experiences in dating lunar impact breccias mentioned in the introduction. With very few exceptions, only molten materials can be used to date impact events whereas whole rock ages of non-molten materials often reflect the pre-impact crystallisation age of the rock or else may yield chronologically insignificant mixing ages (Bogard et al., 1981).

The principal result of the Ries study was already reported in a short communication (Jessberger et al., 1978a). Here, we focus on the post-impact temperature history of the samples within the suevite layer based on the absence of <sup>40</sup>Ar loss from hornblende and on the moderate losses from biotite. We attempt to estimate the maximum temperature experienced by the samples after their formation 320 m.y. ago.

The glass samples have evidently been molten during the impact. Thus local zones of the ejecta layer must have been very hot (~2,000° C). However, the typical dimensions of such hot spots must have been small enough to allow very fast cooling, thereby heating the surrounding rock fragments. If the minerals in these fragments retained essentially all their pre-impact radiogenic <sup>40</sup>Ar, as is the case for hornblende, or if they were only partially degassed, as in the case of biotite, then it becomes possible to deduce the equilibrium temperature experienced by the fragments from their Ar-retention properties.

K–Ar dating of biotite and hornblende from metamorphic contact zones has revealed a substantially greater thermal stability of hornblende as compared to biotite (Dallmeyer, 1975; Hanson et al., 1975). The nearly identical plateau ages obtained in the present study for biotite and hornblende mineral separates provide strong evidence that the equilibrium temperature associated with the impact did not exceed the biotite stability temperature, neither in the suevite layer within the Ries crater, nor in the excavated material. An extreme upper limit for the equilib-

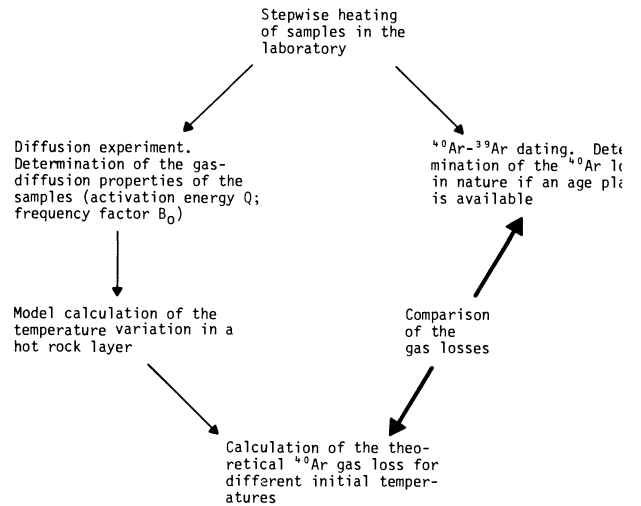


**Fig. 4.** Logical scheme for deducing the initial temperature of the fallback suevite layer (see also Fig. 8)

rium temperature is provided directly by the experimental data: The breccias have not been heated for longer than one hour to the furnace temperature of the first plateau fractions which ranges from 770° C–1,020° C (listed in Table 4 as  $T_{plat}$ ).

To extract a more restricted upper limit we make use of the argon diffusion characteristic of the dated samples in taking the stepwise degassing experiment as a diffusion experiment. Basically, we compare the *measured* loss of <sup>40</sup>Ar after 320 m.y. or the absence of such a loss, if applicable, with the expected <sup>40</sup>Ar loss *calculated* from the Ar diffusion parameters and from a model of the cooling history of the suevite layer in which the initial temperature serves as a free parameter. Then the actual initial temperature results from the fit of the calculated and the measured gas losses (Fig. 4).

The measured quantities  $F_i$  are the cumulative fractions of <sup>40</sup>Ar released after  $i$  degassing steps. From

$$F_i = \frac{6}{\pi^{3/2}} (Bt)_i^{1/2} - \frac{3}{\pi^2} (Bt)_i \quad (0 \leq F_i \leq 0.85) \quad (\text{Reichenberg, 1953}) \quad (1)$$

with  $(Bt)_i = \sum_{n=1}^i B_n t_n$  follows

$$B_i = \frac{(Bt)_i - (Bt)_{i-1}}{t_i} \quad (\text{Evernden et al., 1960})$$

The deduced values for  $\ln(B_i)$  are plotted vs.  $1/T$  in Arrhenius graphs from which the diffusion parameters  $B_0$  and  $Q$  can be extracted as ordinate intercept and slope, respectively (Fig. 5). The following notations are used:

$$B_0 = D_0 \frac{\pi^2}{a^2}; \quad D = D_0 \exp(-Q/RT);$$

and

$$B_n = D_n \frac{\pi^2}{a^2}; \quad D_n = D_0 \exp(-Q/RT_n)$$

$D_0$  = frequency factor;  $a$  = effective diffusion length;  $Q$  = activation energy;  $T$  = temperature;  $t$  = diffusion time;  $i$  = step number.

The resulting parameters should describe the diffusion behaviour of the sample in nature provided that the neutron-irradiation

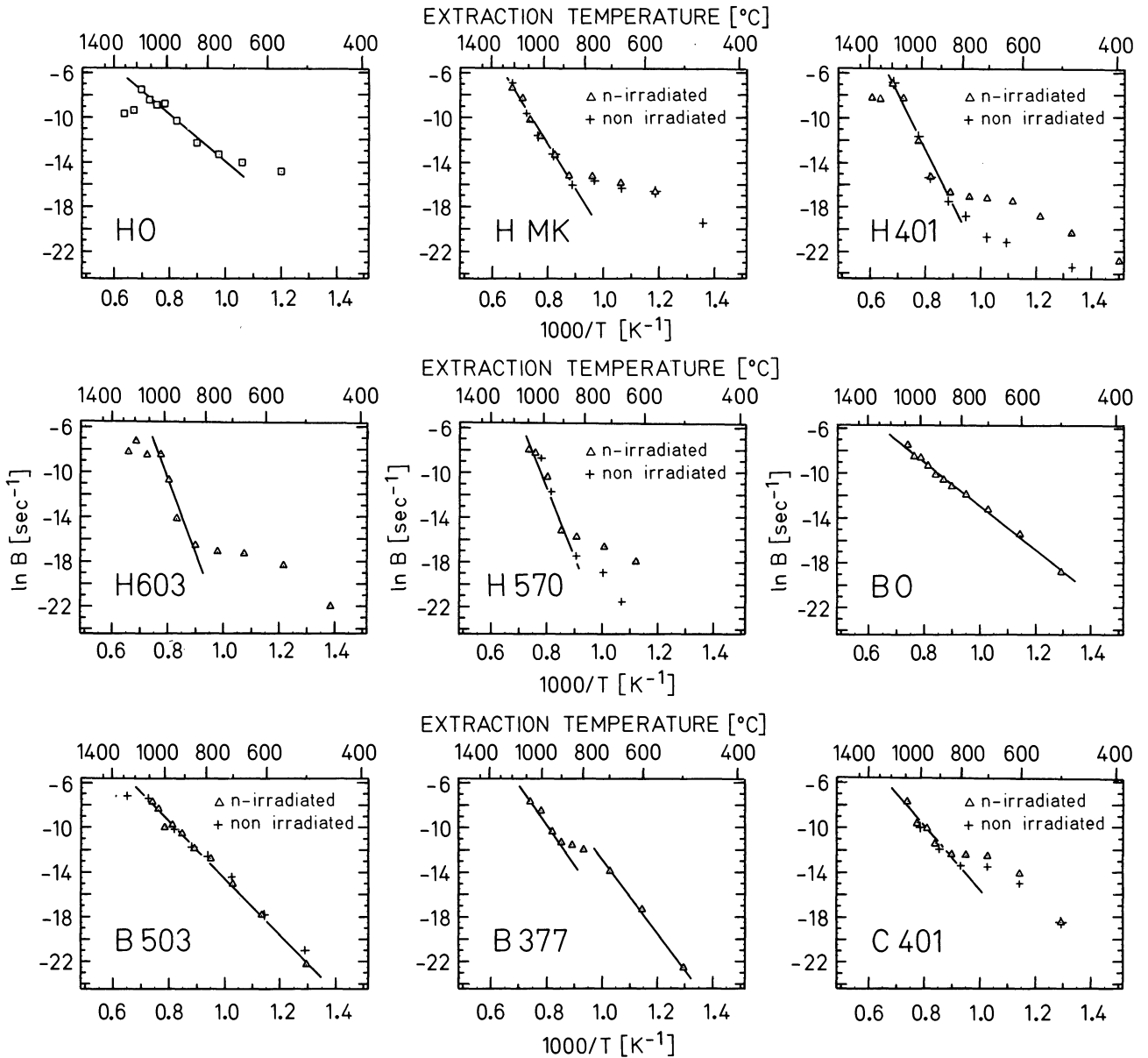


Fig. 5. Arrhenius diagrams for nine mineral separates. For some samples, non-irradiated aliquots have been measured to assure that the neutron-irradiation did not influence the diffusion properties. Extrapolation yields ordinate intercepts  $B_0$ . Activation energies  $Q$  are deduced from the slopes. Both  $B_0$  and  $Q$  are given in Table 4

in the reactor has had no effect. To test this prerequisite we have performed stepwise extractions of non-irradiated aliquots for a number of mineral separates. The respective Arrhenius graphs for both, irradiated and non-irradiated samples, are shown in Fig. 5. In the plateau regions above  $800^\circ\text{C}$  there are no obvious discrepancies between the two. This implies that the applied neutron dose,  $\sim 7 \cdot 10^{16} \text{ n/cm}^2$ , did not change the diffusion parameters for those phases which degas their Ar in the plateau region. The result does not contradict our earlier finding (Horn et al., 1975) that more than  $10^{18} \text{ n/cm}^2$  strongly influence the gas release curve of argon.

The diffusion parameters are calculated using the measured amount of  $^{40}\text{Ar}$  released in the laboratory. If the Arrhenius graph indicates two release regimes we have used only that regime which corresponds to the age plateau and inferred the diffusion constant  $B(T)$  by extrapolation to lower temperatures. If we take into account the natural loss of  $^{40}\text{Ar}$  or else perform

the diffusion calculation with  $^{39}\text{Ar}$ , the resulting low temperature values of  $B(T)$  are always higher, in some cases by orders of magnitude. Higher  $B(T)$  results in faster diffusional loss at low temperatures in the ejecta layer. High  $B(T)$  values from  $^{39}\text{Ar}$  might be due to diffusion, e.g. along grain boundaries. There is also no guarantee that the low temperature portion of the gas release is not influenced by the sample preparation procedure (Gentner and Kley, 1957) or the presence of impurities (cf. samples HO and H585). Consequently, we find it safe to extract the diffusion parameters from those portions of the release where we surely degas pure and undisturbed biotite and hornblende, respectively, that is, the age- and K/Ca-plateau portions. Because of these considerations, the later inferred equilibrium temperatures are upper limits only.

For the temperature history of the cooling layer we assume a constant temperature  $T_0$  of the hot layer immediately after its deposition, initially  $0^\circ\text{C}$  at its base, and  $0^\circ\text{C}$  at its top bound-

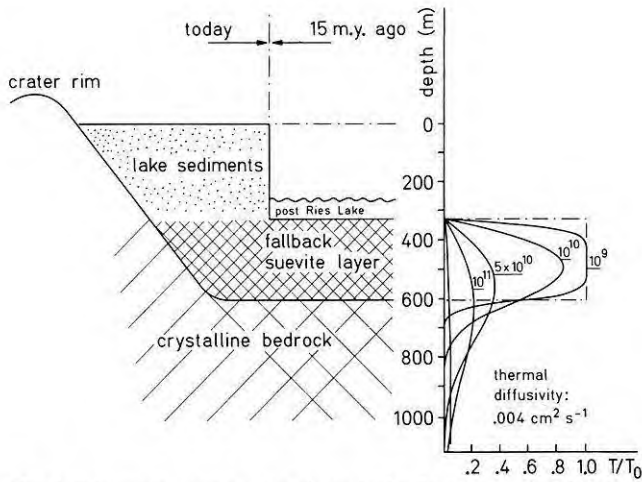


Fig. 6. Schematic cross section through the Ries crater (left hand side) and the corresponding temperature distribution as a function of time, calculated with a thermal diffusivity of  $0.004 \text{ cm}^2/\text{s}$ . The time is given in seconds ( $10^9 \text{ s} \approx 32 \text{ years}$ )

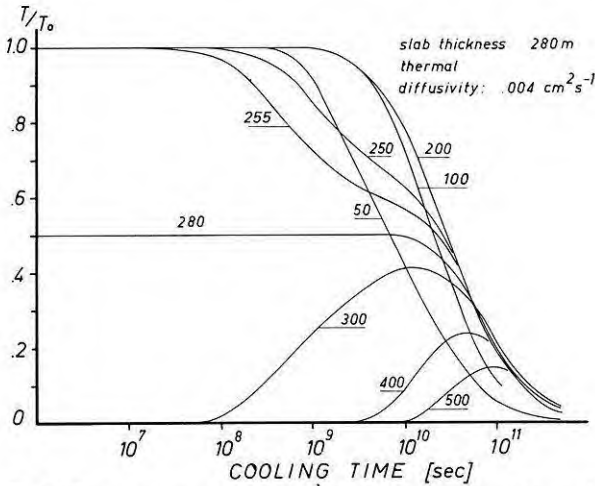


Fig. 7. Temperature evolution for different locations within and below the hot suevite layer. Numerals are the depths in meters below the surface of the suevite layer

ary throughout. Using the solution of the heat diffusion equation for these boundary conditions given by Carslaw and Jäger (1959)

$$T(x, t) = \frac{1}{2} T_0 \left[ 2 \operatorname{erf} \left( \frac{x}{y} \right) - \operatorname{erf} \left( \frac{x+d}{y} \right) - \operatorname{erf} \left( \frac{x-d}{y} \right) \right]$$

$$\text{with } y = \sqrt{4Kt} \quad (2)$$

we obtain the temperature profiles at later times (Fig. 6) as well as the temperature history at given depths within the layer (Fig. 7). In this notation, temperature ( $^{\circ}\text{C}$ ) is expressed in units of  $T/T_0$ ,  $x$  is the depth below the top of the hot slab,  $K$  is the thermal diffusivity of dry Ries suevite,  $0.004 \text{ cm}^2/\text{s}$  (Pohl, 1977), and  $d$  is the slab thickness, taken to be 280 m. For the ejecta blanket samples from outside the crater (HMK, HO, BO)  $d$  is assumed, for simplicity, to be 10 m, although we note that the thickness varies between 12 and 20 m at Otting and is unknown at Meyer's Keller.

Next, the calculation of the gas loss from a sample in a cooling layer is performed by using the diffusion properties ( $B_0$  and  $Q$ ) and the temperature as a function of time at the position of the sample within the layer. The cooling curves (Fig. 7) are

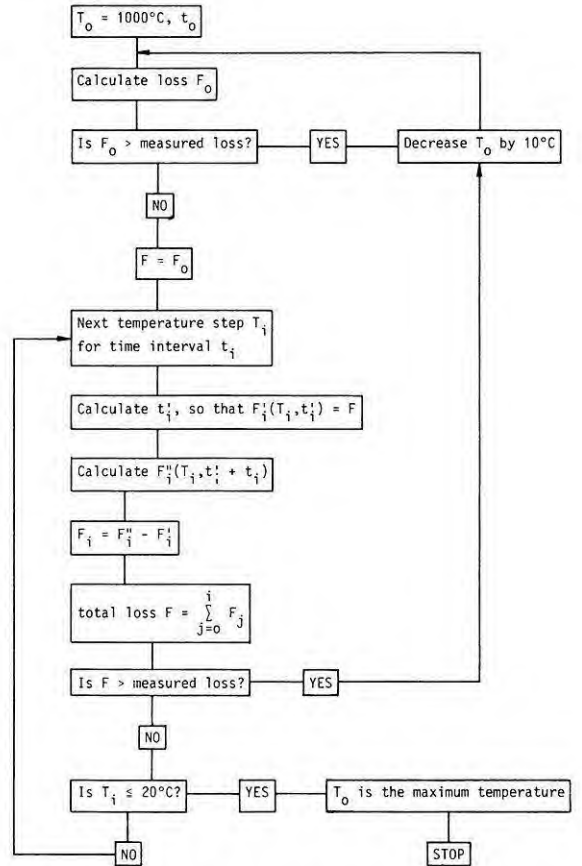


Fig. 8. Flow chart describing the computation of argon loss from minerals within a cooling layer and the determination of the initial temperature by comparison with measured gas losses

approximated by step functions, taking the average of two neighboring temperatures  $T_i = 0.5 (T^{i-1} + T^i)$  where  $T^i$  and  $T^{i-1}$  are separated by time  $t$ . To facilitate the calculation we decided to use time segments which increase according to

$$t_i = 10^6 \sum_{n=1}^i n [\text{s}].$$

In principle, one could now calculate the gas loss for subsequent temperatures  $T_i$  and degassing times  $t_i$  according to the following solutions of Eq. (1):

$$F_i = \frac{6}{\pi^{3/2}} (B_i t_i)^{1/2} - \frac{3}{\pi^2} (B_i t_i) \quad B_i t_i \leq 1$$

$$F_i = 1 - \frac{6}{\pi^2} \exp(-B_i t_i) \quad B_i t_i > 1.$$

However, before calculating the gas loss in the second step ( $i+1$ ), the gas loss of the first step ( $i$ ) has to be taken into account. With an initially homogeneous gas distribution within the mineral, the near surface sites will be more depleted in  $^{40}\text{Ar}$  than the interior sites after the first step. To approximate this situation, we calculate an apparent time  $t^i$ , which is the time required to produce the same  $^{40}\text{Ar}$  loss at the lower temperature  $T_{i+1}$  as would occur within  $t_i$  at  $T_i$  (see Fig. 8). The apparent time  $t^i$  is derived from the previous equation by solving for  $B_i t_i$  and dividing the result by the diffusion parameter  $B_i = B_0 \exp(-Q/R T_{i+1})$ . The gas loss in the second step can now be calculated for the time  $t_{i+1} = t^i + \Delta t_{i+1}$  at the temperature  $T_{i+1}$ .  $\Delta t_{i+1}$  is the time required for the hot slab to cool from  $T^i$  to  $T^{i+1}$ . This stepwise calculation is done as long as the sample releases

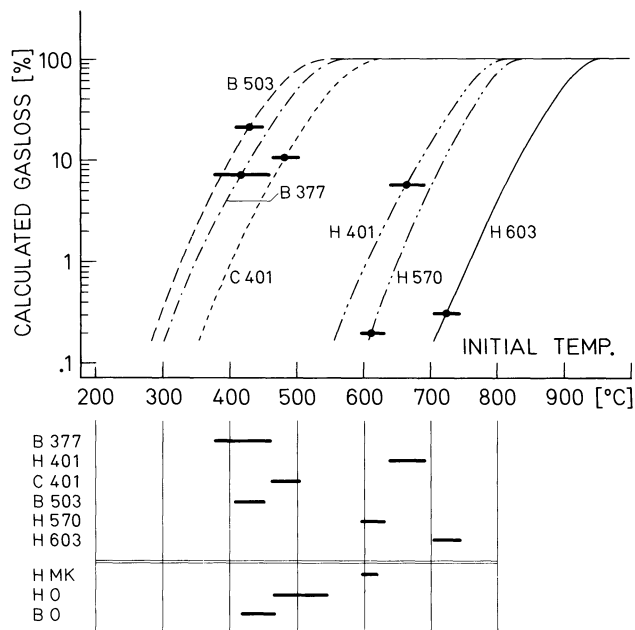


**Fig. 9.** The curves in the upper portion give the calculated gas loss of six mineral separates as a function of the initial temperature if the samples are cooled down in their specific location. Bars indicate the  $^{40}\text{Ar}$  gas loss for these samples, determined from the  $^{40}\text{Ar}$ - $^{39}\text{Ar}$  age spectra and the range for the initial temperature as given in Table 4. The lower part depicts the initial temperature ranges for six core and three surface samples

$^{40}\text{Ar}$ . It will end if either the sample is totally degassed or the temperature in the model is sufficiently low that subsequent  $^{40}\text{Ar}$  losses become insignificant.

The last step in estimating the initial temperature in the suevite layer is to compare the calculated  $^{40}\text{Ar}$ -loss and the natural gas loss determined by the  $^{40}\text{Ar}$ - $^{39}\text{Ar}$  dating experiment. The upper portion of Fig. 9 summarizes the results. The curves represent the relation of the gas loss during cooling from initial temperatures between 900° C and 300° C. Also indicated are the measured  $^{40}\text{Ar}$ -losses for the suevite samples as obtained from the age spectra (Table 3).

The results of our calculations are shown in Fig. 9 (bottom). As mentioned before, the calculated initial temperatures are strictu sensu *maximum* equilibrium temperatures. For example, for the amphibolite from 401 m depth, the hornblende data indicate an initial temperature of  $\sim 670^\circ\text{C}$ , while the data from the chlorite enriched sample C401 yield  $\sim 480^\circ\text{C}$ . Consequently, it must be concluded that  $480^\circ\text{C}$  was the maximum equilibrium temperature at this depth. C401 would have been totally degassed with an initial temperature of  $\geq 550^\circ\text{C}$ . It may be worth mentioning that these different upper temperature limits for the different minerals cannot be regarded as "disagreement" but are fully consistent. The differences simply reflect differences of the response sensitivity of the minerals in the temperature range of interest. Uncontaminated hornblende has almost no  $^{40}\text{Ar}$ -loss, and this corresponds to expectations for temperatures up to a maximum of  $670^\circ\text{C}$  but, of course, the temperature could have been lower as it is in fact the case by inference from the biotite data.

The narrow range of the initial temperatures obtained for samples from various depth (B377, C401, and B503) suggests that the material involved in the formation of the suevite, if it was not totally molten, as a whole did only experience the rather low temperature of about  $450^\circ\text{C}$ . Hence, this temperature

must be regarded as the *average* equilibrium temperature after deposition of the ejecta.

There is ample evidence that dating mono-mineralic portions of impact generated rocks either yield the impact age if the rock had been totally degassed (this study, lunar felsites 73215 and 73255; Scandinavian crater melt rocks: Bottomley et al., 1978; Jessberger and Reimold, 1980; Müller and Jessberger, 1981), or a high temperature plateau age which corresponds to the time of pre-impact crystallisation (this study; Jessberger et al., 1974; Jessberger, 1979). If, however, whole rock samples are dated, the complex argon release behaviour of differently degassed minerals might obscure simple age patterns due to superposition. Then the low and high temperature ages have to be interpreted in terms of upper and lower limits, respectively (Jessberger et al., 1976). This consideration removes the apparent discrepancy between the results obtained in this study and those by Bogard et al. (1981). These authors obtained isochron ages between 19.7 m.y. and 27 m.y. (if two-point "isochrons" are neglected) and a plateau age of 292 m.y. Their result for a whole rock sample from Otting, 20.2 m.y., has, in particular, to be compared to our plateau ages of 311 m.y. and 323 m.y. for hornblende and biotite, respectively. Besides biotite and hornblende, their material contained shock-fused feldspar as the major K-bearing phase. In a recent experiment (Jessberger and Ostertag, in press 1982) we have demonstrated that up to at least 450 kbar, probably up to 525 kbar, shock-effects on the K-Ar clock of feldspar are as minimal as they are on biotite and hornblende, as shown in this study. So it is again concluded that only molten materials give an age similar to the age of the Ries event, 15 m.y. (Table 3).

In a joint effort with the  $^{40}\text{Ar}$ - $^{39}\text{Ar}$  experiments, Wagner and Miller (1978) performed a fission track study of minerals from the Ries drill core. Their data can be treated in a manner analogous to the argon data. The degree of track fading corresponds to the amount of argon loss. For a sphene from 377 m depth and an apatite from 585 m depth the observed degrees of track fading are 70% and 60%, respectively. Using track annealing properties of these minerals (sphene: Naeser and Faul, 1969; apatite: Wagner, private communication) and the cooling diagram of Fig. 7, we arrive at maximum initial temperatures of  $480^\circ\text{C}$  at 377 m (deduced from sphene) and  $240^\circ\text{C}$  at 585 m (deduced from apatite). This strongly corroborates the estimates inferred from the argon study. The agreement of the temperatures inferred from sphene and biotite B377, both from the same depth, makes it probable that the deduced maximum equilibrium temperature of the high temperature suevite layer is in fact the *true* temperature to which these rocks were exposed. The maximum temperature for the lower suevite layer is given by the apatite data to be about  $250^\circ\text{C}$ .

An estimate of minimum temperatures stems from paleomagnetic data. Pohl (1977) found that in the high temperature suevite layer the temperature exceeded the Curie temperature of magnetite,  $580^\circ\text{C}$ , that is, about  $130^\circ\text{C}$  above the estimates from the argon and the track data. The discrepancy may be due to a cooling of the suevite layer much faster than assumed in our model, e.g. due to groundwater penetrating the layer. The heat diffusivity used in the cooling model applies for dry suevite only (Pohl, 1977). We have performed calculations of the initial temperature for a wide range of heat diffusivities (K from 0.004 to  $0.8\text{ cm}^2/\text{s}$ ). They show that, e.g. for sample B377, an increase of K by two orders of magnitude would result in a  $95^\circ\text{C}$  increase of the initial temperature (from  $420^\circ\text{C}$  to  $515^\circ\text{C}$ ). For the biotite from Otting, the same increase of K would rise the initial temperature from  $445^\circ\text{C}$  to  $590^\circ\text{C}$ .

## Summary

1) The age of the Nördlinger Ries impact, obtained from a moldavite and an impact glass sample, has been confirmed to be  $15.1 \pm 0.1$  m.y.

2) The K–Ar systems in hornblende and biotite are remarkably stable against shock pressures of up to 450 kbar.

3) The common plateau age of the mineral separates from drill core samples as well as from ejecta rocks dates the Ries bedrock to be 320 m.y. old.

4) From the argon data as well as from fission track data (Wagner and Miller, 1978) a maximum average equilibrium temperature of about 450° C is inferred for the upper fallback suevite layer and the fallout suevite, and about 250° C for the lower fallback suevite.

*Acknowledgements.* The authors are indebted to G. Wagner, D. Stöffler, and an anonymous reviewer for helpful suggestions, discussions, and critical comments. This work has been supported by the Gesellschaft für Kernforschung mbH, Karlsruhe.

## References

- Bauberger, W., Mielke, H., Schmeer, D., Stettner, G.: Petrographische Profildarstellung der Forschungsbohrung Nördlingen 1973. *Geol. Bavarica* **72**, 33–34, 1974
- Bogard, D.D., Hörz, F., Johnson, P., Stöffler, D.: Resetting of  $^{40}\text{Ar}/^{39}\text{Ar}$  ages in suevite ejecta from the Ries crater. *Lunar Planet. Sci. Conf.* **12**, 92, 1981
- Bottomley, R.J., York, D., Grieve, R.A.F.:  $^{40}\text{Ar}$ – $^{39}\text{Ar}$  ages of Scandinavian impact structures: I Mien and Siljan. *Contrib. Mineral. Petrol.* **68**, 79–84, 1978
- Carlsaw, H.S., Jaeger, J.C.: Conduction of heat in solids. Oxford Clarendon Press 1959
- Dallmeyer, R.D.:  $^{40}\text{Ar}/^{39}\text{Ar}$  ages of biotite and hornblende from a progressively remetamorphosed basement terrane: Their bearing on interpretation of release spectra. *Geochim. Cosmochim. Acta* **39**, 1655–1669, 1975
- El Goresy, A., Chao, E.C.T.: Discovery, origin and significance of Fe–Cr–Ni veinlets in the compressed zone of the Ries research drill core. *Geol. Bavarica* **75**, 229–296, 1977
- Engelhardt, W.v., Graup, G.: Stoßwellenmetamorphose im Kristallin der Forschungsbohrung Nördlingen 1973. *Geol. Bavarica* **75**, 255–271, 1977
- Evernden, J.F., Curtis, G.H., Kistler, R.W., Obradovich, J.: Argon diffusion in glauconite, microcline, sanidine, leucite and phlogopite. *Am. J. Sci.* **258**, 583, 1960
- Gentner, W., Kley, O.: Argonbestimmungen an Kaliummineralien – IV Die Frage der Argonverluste in Kalifeldspäten und Glimmermineralien. *Geochim. Cosmochim. Acta* **12**, 323–329, 1957
- Gentner, W., Lippolt, H.J., Schaeffer, O.A.: Das Kalium-Argon-Alter einer Glasprobe vom Nördlinger Ries. *Z. Naturforsch.* **16a**, 11, 1961
- Gentner, W., Storzer, D., Wagner, G.A.: New fission track ages of tektites and related glasses. *Geochim. Cosmochim. Acta* **33**, 1075–1081, 1969
- Graup, G.: Die Petrographie der kristallinen Gesteine der Forschungsbohrung Nördlingen 1973. *Geol. Bavarica* **75**, 219, 1977
- Gudden, H.: Die Forschungsbohrung Nördlingen 1973, Durchführung und erste Befunde. *Geol. Bavarica* **72**, 11–31, 1974
- Hanson, G.N., Simmons, K.R., Bence, A.E.:  $^{40}\text{Ar}/^{39}\text{Ar}$  spectrum ages for biotite, hornblende and muscovite in a contact metamorphic zone. *Geochim. Cosmochim. Acta* **39**, 1269–1277, 1975
- Higuchi, M., Morgan, J.W.: Ancient meteoritic component in Apollo 17 boulders. *Proc. Lunar Sci. Conf.* **6**, 1625–1651, 1975
- Horn, P., Kirsten, T.: Lunar highland stratigraphy and radiometric dating. *Philos. Trans. R. Soc. London* **A285**, 145–150, 1977
- Horn, P., Jessberger, E.K., Kirsten, T., Richter, H.:  $^{39}\text{Ar}$ – $^{40}\text{Ar}$  dating of lunar rocks: Effects of grain size and neutron irradiation. *Proc. Lunar Sci. Conf.* **6**, 1563–1591, 1975
- Jäger, E.: Colloquium on the Geochronology of Phanerozoic Orogenic Belts. Zurich and Bern. Data Compilation in Abstract Volume, 1969
- James, O.B., Blanchard, D.P.: Consortium studies of light gray breccia 73215: Introduction, subsample distribution data and summary of results. *Proc. Lunar Sci. Conf.* **7**, 2131–2143, 1976
- James, O.B., Hammarstrom, J.G.: Petrology of four clasts from consortium breccia 73215. *Proc. Lunar Sci. Conf.* **8**, 2459–2494, 1977
- James, O.B., Hedenquist, J.W., Blanchard, D.P., Budahn, J.R., Compton, W.: Consortium breccia 73255: Petrology, major- and trace-element chemistry, and Rb–Sr systematics of aphanitic lithologies. *Proc. Lunar Planet. Sci. Conf.* **9**, 789–819, 1978
- Jessberger, E.K.: Ancient pink-spinel-bearing troctolitic basalt in Apollo 17 breccia 73215. *Lunar Planet. Sci.* **10**, 625–627. The Lunar and Planetary Institute, Houston, 1979
- Jessberger, E.K., Huneke, J.C., Wasserburg, G.J.: High resolution argon analysis of neutron-irradiated Apollo 16 rocks and separated minerals. *Proc. Lunar Sci. Conf.* **5**, 1419–1449, 1974
- Jessberger, E.K., Kirsten, T., Staudacher, Th.: Argon-argon ages of consortium breccia 73215. *Proc. Lunar Sci. Conf.* **7**, 2201–2215, 1976
- Jessberger, E.K., Kirsten, T., Staudacher, Th.: One rock and many ages – Further K–Ar data on consortium breccia 73215. *Proc. Lunar Sci. Conf.* **8**, 2567–2580, 1977
- Jessberger, E.K., Staudacher, Th., Dominik, B., Kirsten, T., Schaeffer, O.A.: Limited response of the K–Ar system to the Nördlinger Ries giant meteorite impact. *Nature* **271**, 338–339, 1978a
- Jessberger, E.K., Staudacher, Th., Dominik, B., Kirsten, T.: Argon-argon ages of aphanite samples from consortium breccia 73255. *Proc. Lunar Planet. Sci. Conf.* **9**, 841–854, 1978b
- Jessberger, E.K., Reimold, W.U.: A late cretaceous  $^{40}\text{Ar}$ – $^{39}\text{Ar}$  age of the Lappajärvi impact crater, Finland. *J. Geophys.* **48**, 57, 1980
- Jessberger, E.K., Ostertag, R.: Shock effects on the K–Ar system of feldspar and the age of anorthositic inclusions from North-Eastern Minnesota. *Geochim. Cosmochim. Acta*, in press 1982
- Kirsten, T., Horn, P.: Chronology of the Taurus-Littrow Valley III Ages of mare basalts and highland breccias and some remarks about the interpretation of lunar highland rock ages. *Proc. Lunar Sci. Conf.* **5**, 1415–1475, 1975
- Müller, N., Jessberger, E.K.:  $^{40}\text{Ar}$ – $^{39}\text{Ar}$  Datierung skandinavischer Impaktkrater. 41. Jahrestagung der Deutschen-Geophysikalischen Gesellschaft, Heidelberg, 1981 (Abstr.)
- Naeser, C.W., Faul, H.: Fission track annealing in apatite and sphene. *J. Geophys. Res.* **74**, 705–710, 1969
- Pohl, J.: Paläomagnetische und gesteinsmagnetische Untersuchungen an den Kernen der Forschungsbohrung Nördlingen 1973. *Geol. Bavarica* **75**, 329–348, 1977
- Reichenberg, D.: Properties of ion-exchange resins in relation to their structure, III. Kinetics of exchange. *Am. Chem. Soc.* **75**, 589, 1953
- Ryder, D., Wood, J.A.: Serenitatis and Imbrium impact melts: Implications for large scale layering in the lunar crust. *Proc. Lunar Sci. Conf.* **8**, 655–668, 1977
- Schaeffer, O.A., Husain, L., Schaeffer, G.H.: Ages of highland rocks: The chronology of basin formation revisited. *Proc. Lunar Sci. Conf.* **7**, 2067–2093, 1976
- Schaeffer, O.A., Schaeffer, G.H.:  $^{39}\text{Ar}$ – $^{40}\text{Ar}$  ages of lunar rocks. *Proc. Lunar Sci. Conf.* **8**, 2253–2300, 1977
- Schmidt-Kaler (ed.): Ergebnisse der Ries-Forschungsbohrung 1973: Struktur des Kraters und Entwicklung des Kratersees. *Geol. Bavarica* **75**, 1977
- Staudacher, Th., Jessberger, E.K., Flohs, I., Kirsten, T.:  $^{40}\text{Ar}$ – $^{39}\text{Ar}$  age systematics of consortium breccia 73255. *Proc. Lunar Planet. Sci. Conf.* **10**, 745–762, 1969
- Steiger, R.H., Jäger, E.: Subcommittee on Geochronology: Convention on the use of decay constants in geo- and cosmochronology. *Earth Planet. Sci. Lett.* **36**, 359–362, 1977
- Stöffler, D.: Progressive metamorphism and classification of shocked and brecciated crystalline rocks at impact craters. *J. Geophys. Res.* **76**, 5541–5551, 1971

- Stöffler, D.: Deformation and transformation of rock forming minerals by natural and experimental shock pressures. *Fortschr. Mineral.* **49**, 50–113, 1972
- Stöffler, D., Ewald, D., Ostertag, U., Reimold, W.U.: Research drilling Nördlingen 1973 (Ries): Composition and texture of polymict impact breccias. *Geol. Bavarica* **75**, 163–189, 1977
- Turner, G.: Potassium-argon chronology of the moon. *Phys. Chem. Earth* **10**, 145–195, 1977
- Wagner, G.A., Miller, D.S.: Cooling history of rocks in the Ries crater revealed by fission track analyses. *Proc. IV. Intern. Conf. Geochron. Cosmochron., Isotope Geology*, Aspen, Colorado. Geol. Survey: Open File Report 78–701, 440–442, 1978

Received April 21, 1981; Revised January 4 and February 23, 1982  
Accepted February 25, 1982